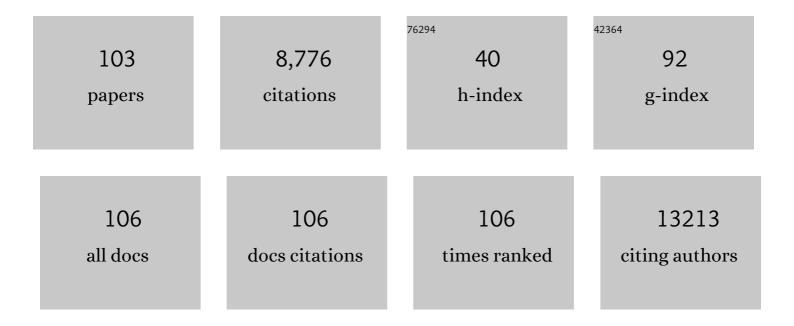
## Long Chen

List of Publications by Year in descending order

Source: https://exaly.com/author-pdf/3118483/publications.pdf Version: 2024-02-01



#	Article	IF	CITATIONS
1	Znâ€doped NiCo <sub>2</sub> O <sub>4</sub> as Modified Electrode Nanomaterials for Enhanced Electrochemical Detection Performance of Cu(II). Electroanalysis, 2022, 34, 1844-1853.	1.5	5
2	One-pot synthesis of CoxSy nanomaterials for high-performance supercapacitors. Journal of Materials Science: Materials in Electronics, 2022, 33, 10013-10020.	1.1	1
3	Hybrid-metal hydroxyl fluoride nanosheet arrays as a bifunctional electrocatalyst for efficient overall water splitting. Journal of Materials Chemistry A, 2022, 10, 11774-11783.	5.2	11
4	Flocculation-to-adsorption transition of novel salt-responsive polyelectrolyte for recycling of highly polluted saline textile effluents. Chemical Engineering Journal, 2021, 413, 127410.	6.6	29
5	Review of ZnO-based nanomaterials in gas sensors. Solid State Ionics, 2021, 360, 115544.	1.3	211
6	ZnFe <sub>2</sub> O <sub>4</sub> Nanoparticles for Electrochemical Determination of Trace Hg(II), Pb(II), Cu(II), and Glucose. ACS Applied Nano Materials, 2021, 4, 4026-4036.	2.4	48
7	Unlocking the dissolution mechanism of phosphorus anode for lithium-ion batteries. Energy Storage Materials, 2021, 37, 417-423.	9.5	36
8	Bacterial cytoplasmic membranes synergistically enhance the antitumor activity of autologous cancer vaccines. Science Translational Medicine, 2021, 13, .	5.8	109
9	Tunable nitrogen-doped delaminated 2D MXene obtained by NH3/Ar plasma treatment as highly efficient hydrogen and oxygen evolution reaction electrocatalyst. Chemical Engineering Journal, 2021, 420, 129832.	6.6	30
10	Evaluation of renewable pH-responsive starch-based flocculant on treating and recycling of highly saline textile effluents. Environmental Research, 2021, 201, 111489.	3.7	17
11	Oxygen vacancies enriched nickel cobalt based nanoflower cathodes: Mechanism and application of the enhanced energy storage. Journal of Energy Chemistry, 2021, 62, 252-261.	7.1	54
12	Synthesis and electrocatalytic mechanism of ultrafine MFe <sub>2</sub> O <sub>4</sub> (M: Co, Ni, and) Tj ETQ and hydrogen evolution reaction performances. Journal of Materials Chemistry A, 2021, 9, 22277-22290.	990 0 0 rgB 5.2	T /Overlock ] 26
13	Crystalline-Amorphous Hybrid CoNiO <sub>2</sub> Nanowires with Enhanced Capacity and Energy Density for Aqueous Zinc-Ion Hybrid Supercapacitors. ACS Applied Energy Materials, 2021, 4, 12345-12352.	2.5	11
14	Overwhelming electrochemical oxygen reduction reaction of zinc-nitrogen-carbon from biomass resource chitosan via a facile carbon bath method. Chinese Chemical Letters, 2020, 31, 1207-1212.	4.8	13
15	Walnut shell-derived hierarchical porous carbon with high performances for electrocatalytic hydrogen evolution and symmetry supercapacitors. International Journal of Hydrogen Energy, 2020, 45, 443-451.	3.8	55
16	Fast and facile preparation of S nanoparticles by flash nanoprecipitation for lithium–sulfur batteries. New Journal of Chemistry, 2020, 44, 466-471.	1.4	5
17	Polyoxometalate intercalated NiFe layered double hydroxides for advanced water oxidation. International Journal of Hydrogen Energy, 2020, 45, 1802-1809.	3.8	37
18	Continuous Surface Strain Tuning for NiFe-Layered Double Hydroxides Using a Multi-inlet Vortex Mixer. Industrial & Engineering Chemistry Research, 2020, 59, 19897-19906.	1.8	0

#	Article	IF	CITATIONS
19	Chemical vapor deposition of layered two-dimensional MoSi <sub>2</sub> N <sub>4</sub> materials. Science, 2020, 369, 670-674.	6.0	556
20	CdPS <sub>3</sub> nanosheets-based membrane with high proton conductivity enabled by Cd vacancies. Science, 2020, 370, 596-600.	6.0	120
21	Synthesis of Co2â^'xNixO2 (0 < x < 1.0) hexagonal nanostructures as efficient bifunctional electrocatalysts for overall water splitting. Dalton Transactions, 2020, 49, 6587-6595.	1.6	20
22	A cellulose dissolution and encapsulation strategy to prepare carbon nanospheres with ultra-small size and high nitrogen content for the oxygen reduction reaction. New Journal of Chemistry, 2020, 44, 10613-10620.	1.4	7
23	In Situ Formation of NiAl-Layered Double Hydroxide with a Tunable Interlayer Spacing in a Confined Impinging Jet Microreactor. Energy & Fuels, 2020, 34, 8939-8946.	2.5	9
24	Au–Ag alloy nanoparticles with tunable cavity for plasmon-enhanced photocatalytic H2 evolution. Journal of Energy Chemistry, 2020, 49, 1-7.	7.1	42
25	Uniformly dispersed Fe3C (~5 nm) in Fe-N-doped carbon nanosheets derived from coal tar pitch as efficient electrocatalysts for oxygen reduction reaction. Materials Letters, 2020, 273, 127861.	1.3	7
26	Boosting the Potassium-Ion Storage Performance in Soft Carbon Anodes by the Synergistic Effect of Optimized Molten Salt Medium and N/S Dual-Doping. ACS Applied Materials & Interfaces, 2020, 12, 20838-20848.	4.0	88
27	Flocculant-Assisted Synthesis of Graphene-Like Carbon Nanosheets for Oxygen Reduction Reaction and Supercapacitor. Nanomaterials, 2019, 9, 1135.	1.9	10
28	Preparation of mesoporous CoNiO2 hexagonal nanoparticles for asymmetric supercapacitors via a hydrothermal microwave carbon bath process. New Journal of Chemistry, 2019, 43, 15066-15071.	1.4	4
29	N, S Dual-Doped Carbon Derived from Dye Sludge by Using Polymeric Flocculant as Soft Template. Nanomaterials, 2019, 9, 991.	1.9	4
30	Hierarchical CoNiO2 polyhedral mesoporous nanoparticles: Hydrothermal microwave carbon bath process synthesis and ultrahigh electrochemical activity for detection of Cu(II). Electrochimica Acta, 2019, 320, 134581.	2.6	9
31	High efficiency and fast van der Waals hetero-photodiodes with a unilateral depletion region. Nature Communications, 2019, 10, 4663.	5.8	213
32	Tunable In Situ Stress and Spontaneous Microwrinkling of Multiscale Heterostructures. Journal of Physical Chemistry C, 2019, 123, 26041-26046.	1.5	3
33	Bottom-Up Synthesis of 2D Transition Metal Carbides and Nitrides. , 2019, , 89-109.		13
34	AsP/InSe Van der Waals Tunneling Heterojunctions with Ultrahigh Reverse Rectification Ratio and High Photosensitivity. Advanced Functional Materials, 2019, 29, 1900314.	7.8	121
35	One-step synthesis of nickel–iron layered double hydroxides with tungstate acid anions <i>via</i> flash nano-precipitation for the oxygen evolution reaction. Sustainable Energy and Fuels, 2019, 3, 237-244.	2.5	45
36	Cu-Doped Porous Carbon Derived from Heavy Metal-Contaminated Sewage Sludge for High-Performance Supercapacitor Electrode Materials. Nanomaterials, 2019, 9, 892.	1.9	15

#	Article	IF	CITATIONS
37	High efficient oxygen reduction performance of Fe/Fe3C nanoparticles in situ encapsulated in nitrogen-doped carbon via a novel microwave-assisted carbon bath method. Nano Materials Science, 2019, 1, 131-136.	3.9	9
38	N-doped Carbon Coated CoO Nanowire Arrays Derived from Zeolitic Imidazolate Framework-67 as Binder-free Anodes for High-performance Lithium Storage. Scientific Reports, 2019, 9, 5934.	1.6	12
39	Synthesis and formation mechanism of monodisperse Mn-Co-Ni-O spinel nanocrystallines. Advanced Powder Technology, 2019, 30, 1269-1276.	2.0	6
40	Transport Properties of Topological Semimetal Tungsten Carbide in the 2D Limit. Advanced Electronic Materials, 2019, 5, 1800839.	2.6	5
41	Nitrogen self-doped porous carbon nanosheets derived from azo dye flocs for efficient supercapacitor electrodes. Carbon Letters, 2019, 29, 455-460.	3.3	3
42	Designed formation of NiCo2O4 with different morphologies self-assembled from nanoparticles for asymmetric supercapacitors and electrocatalysts for oxygen evolution reaction. Electrochimica Acta, 2019, 296, 719-729.	2.6	86
43	Highly stable graphene-oxide-based membranes with superior permeability. Nature Communications, 2018, 9, 1486.	5.8	428
44	Amphoteric starch derivatives as reusable flocculant for heavy-metal removal. RSC Advances, 2018, 8, 1274-1280.	1.7	26
45	Nitrogen and Sulfur Self-Doped Activated Carbon Directly Derived from Elm Flower for High-Performance Supercapacitors. ACS Omega, 2018, 3, 4724-4732.	1.6	122
46	Facile one-step fabrication of CdS <sub>0.12</sub> Se <sub>0.88</sub> quantum dots with a ZnSe/ZnS-passivation layer for highly efficient quantum dot sensitized solar cells. Journal of Materials Chemistry A, 2018, 6, 9866-9873.	5.2	38
47	pH-responsive chitosan-based flocculant for precise dye flocculation control and the recycling of textile dyeing effluents. RSC Advances, 2018, 8, 39334-39340.	1.7	20
48	Thermo- and pH-responsive starch derivatives for smart window. Carbohydrate Polymers, 2018, 196, 209-216.	5.1	18
49	Three-Dimensional Honeycomb-Like Porous Carbon with Both Interconnected Hierarchical Porosity and Nitrogen Self-Doping from Cotton Seed Husk for Supercapacitor Electrode. Nanomaterials, 2018, 8, 412.	1.9	52
50	NiPS <sub>3</sub> Nanosheet–Graphene Composites as Highly Efficient Electrocatalysts for Oxygen Evolution Reaction. ACS Nano, 2018, 12, 5297-5305.	7.3	104
51	Circular Graphene Platelets with Grain Size and Orientation Gradients Grown by Chemical Vapor Deposition. Advanced Materials, 2017, 29, 1605451.	11.1	8
52	One-Step Device Fabrication of Phosphorene and Graphene Interdigital Micro-Supercapacitors with High Energy Density. ACS Nano, 2017, 11, 7284-7292.	7.3	312
53	Strongly Coupled High-Quality Graphene/2D Superconducting Mo <sub>2</sub> C Vertical Heterostructures with Aligned Orientation. ACS Nano, 2017, 11, 5906-5914.	7.3	110
54	Grafting heteroelement-rich groups on graphene oxide: Tuning polarity and molecular interaction with bio-ionic liquid for enhanced lubrication. Journal of Colloid and Interface Science, 2017, 498, 47-54.	5.0	19

#	Article	IF	CITATIONS
55	Pore size dependent molecular adsorption of cationic dye in biomass derived hierarchically porous carbon. Journal of Environmental Management, 2017, 196, 168-177.	3.8	29
56	Effect of Microbial-Induced Calcite Precipitation on Surface Erosion and Scour of Granular Soils. Transportation Research Record, 2017, 2657, 10-18.	1.0	20
57	Effect of sintering temperature on thermal stability of Zn0.2Fe1.05NiMn0.75O4 ceramic materials by homogeneous co-precipitation method. Journal of Materials Science: Materials in Electronics, 2017, 28, 190-196.	1.1	5
58	Fabrication and thermosensitive characteristics of BaCoO3â~ĺ ceramics for low temperature negative temperature coefficient thermistor. Journal of Materials Science: Materials in Electronics, 2017, 28, 6239-6244.	1.1	7
59	Phosphorene as a Polysulfide Immobilizer and Catalyst in Highâ€Performance Lithium–Sulfur Batteries. Advanced Materials, 2017, 29, 1602734.	11.1	289
60	Cotton fabric derived hierarchically porous carbon and nitrogen doping for sustainable capacitor electrode. Carbon, 2017, 111, 839-848.	5.4	140
61	Direct observation of the layer-dependent electronic structure in phosphorene. Nature Nanotechnology, 2017, 12, 21-25.	15.6	625
62	Formation of Mnâ€Coâ€Niâ€O Nanoceramic Microspheres Using In Situ Inkâ€Jet Printing: Sintering Process Effect on the Microstructure and Electrical Properties. Small, 2016, 12, 5027-5033.	5.2	24
63	Scalable Clean Exfoliation of Highâ€Quality Few‣ayer Black Phosphorus for a Flexible Lithium Ion Battery. Advanced Materials, 2016, 28, 510-517.	11.1	336
64	Magnetotransport Properties in High-Quality Ultrathin Two-Dimensional Superconducting Mo <sub>2</sub> C Crystals. ACS Nano, 2016, 10, 4504-4510.	7.3	69
65	Paving the Thermal Highway with Self-Organized Nanocrystals in Transparent Polymer Composites. ACS Applied Materials & Interfaces, 2016, 8, 29080-29087.	4.0	35
66	Boosting Energy Efficiency of Nickel Cobaltite via Interfacial Engineering in Hierarchical Supercapacitor Electrode. Journal of Physical Chemistry C, 2016, 120, 23377-23388.	1.5	14
67	High performance of Ni <sub>0.9</sub> Mn <sub>1.8</sub> Mg <sub>0.3</sub> O <sub>4</sub> spinel nanoceramic microbeads via inkjet printing and two step sintering. RSC Advances, 2016, 6, 35118-35123.	1.7	6
68	Preparation and characterization of Mn1.2Co0.6Ni1.2O4 NTC ceramic materials by rheological phase reaction method. Journal of Materials Science: Materials in Electronics, 2016, 27, 12649-12653.	1.1	0
69	Molecular Transformation, Diffusion, and Assembling into Three-Dimensional Freestanding Tube Arrays via a Triphasic Reaction. Langmuir, 2016, 32, 11525-11531.	1.6	0
70	Enriching Heteroelements in Lignin as Lubricating Additives for Bioionic Liquids. ACS Sustainable Chemistry and Engineering, 2016, 4, 3877-3887.	3.2	36
71	Effect of sintering temperature on microstructure and electrical properties of Mn1.2Co1.5Ni0.3O4 ceramic materials using nanoparticles by reverse microemulsion method. Journal of Materials Science: Materials in Electronics, 2016, 27, 1713-1718.	1.1	12
72	Preparation and characterization of LaMn0.5Co0.5O3–Ni0.66Mn2.34O4 composite NTC ceramics. Journal of Materials Science: Materials in Electronics, 2016, 27, 7560-7565.	1.1	7

#	Article	IF	CITATIONS
73	Confined molecular motion across liquid/liquid interfaces in a triphasic reaction towards free-standing conductive polymer tube arrays. Journal of Materials Chemistry A, 2016, 4, 6290-6294.	5.2	7
74	Green processing of plant biomass into mesoporous carbon as catalyst support. Chemical Engineering Journal, 2016, 295, 301-308.	6.6	55
75	Superamphiphobicity and electroactivity enabled dual physical/chemical protections in novel anticorrosive nanocomposite coatings. Polymer, 2016, 85, 37-46.	1.8	46
76	lonic Grease Lubricants: Protic [Triethanolamine][Oleic Acid] and Aprotic [Choline][Oleic Acid]. ACS Applied Materials & Interfaces, 2016, 8, 4977-4984.	4.0	45
77	Heterogeneous nucleation/growth of silver nanoparticles onto oxygenated mesoporous carbon: Alcohol effect and catalytic property. Catalysis Communications, 2016, 77, 65-69.	1.6	8
78	Facile synthesis of mesoporous carbon nanocomposites from natural biomass for efficient dye adsorption and selective heavy metal removal. RSC Advances, 2016, 6, 2259-2269.	1.7	74
79	In-situ reduction of Ag nanoparticles on oxygenated mesoporous carbon fabric: Exceptional catalyst for nitroaromatics reduction. Applied Catalysis B: Environmental, 2016, 182, 306-315.	10.8	68
80	Efficient Perovskite Hybrid Solar Cells via Ionomer Interfacial Engineering. Advanced Functional Materials, 2015, 25, 6875-6884.	7.8	57
81	Multichannel Conductance of Folded Singleâ€Molecule Wires Aided by Throughâ€Space Conjugation. Angewandte Chemie - International Edition, 2015, 54, 4231-4235.	7.2	92
82	Hierarchical Porous and High Surface Area Tubular Carbon as Dye Adsorbent and Capacitor Electrode. ACS Applied Materials & Interfaces, 2015, 7, 12230-12237.	4.0	106
83	High Fluorescence Efficiencies and Large Stokes Shifts of Folded Fluorophores Consisting of a Pair of Alkenyl-Tethered, π-Stacked Oligo- <i>p</i> -phenylenes. Organic Letters, 2015, 17, 6174-6177.	2.4	40
84	Hierarchical macrotube/mesopore carbon decorated with mono-dispersed Ag nanoparticles as a highly active catalyst. Green Chemistry, 2015, 17, 2515-2523.	4.6	114
85	Efficiencies of perovskite hybrid solar cells influenced by film thickness and morphology of CH3NH3PbI3â <sup>~,</sup> xClx layer. Organic Electronics, 2015, 21, 19-26.	1.4	56
86	[N-Methyl-2-pyrrolidone][C1–C4 carboxylic acid]: a novel solvent system with exceptional lignin solubility. Chemical Communications, 2015, 51, 13554-13557.	2.2	36
87	Non-corrosive green lubricants: strengthened lignin–[choline][amino acid] ionic liquids interaction via reciprocal hydrogen bonding. RSC Advances, 2015, 5, 66067-66072.	1.7	68
88	Phase transition and electrical properties of Ni1â^'x Zn x Mn2O4 (0Ââ‰ <b>¤̂</b> xÂâ‰ <b>¤̂</b> 1.0) NTC ceramics. Journal of Materials Science: Materials in Electronics, 2015, 26, 1374-1380.	1.1	22
89	Carbon monolith with embedded mesopores and nanoparticles as a novel adsorbent for water treatment. RSC Advances, 2015, 5, 42540-42547.	1.7	17
90	Superhydrophobic polyaniline hollow spheres with mesoporous brain-like convex-fold shell textures. Journal of Materials Chemistry A, 2015, 3, 19299-19303.	5.2	28

#	Article	IF	CITATIONS
91	Large-area high-quality 2D ultrathin Mo2C superconducting crystals. Nature Materials, 2015, 14, 1135-1141.	13.3	1,045
92	Unveiling Mesopore Evolution in Carbonized Wood: Interfacial Separation, Migration, and Degradation of Lignin Phase. ACS Sustainable Chemistry and Engineering, 2015, 3, 2489-2495.	3.2	21
93	Synthesis and characterization of Mn–Co–Ni–O ceramic nanoparticles by reverse microemulsion method. Ceramics International, 2015, 41, 2847-2851.	2.3	27
94	2,5â€Ðifluorenylâ€Substituted Siloles for the Fabrication of Highâ€Performance Yellow Organic Lightâ€Emitting Diodes. Chemistry - A European Journal, 2014, 20, 1931-1939.	1.7	58
95	Fabrication and properties of Mn1.56Co0.96Ni0.48O4 free-standing ultrathin chips. Ceramics International, 2014, 40, 8405-8409.	2.3	41
96	Creation of Bifunctional Materials: Improve Electronâ€Transporting Ability of Light Emitters Based on AlEâ€Active 2,3,4,5â€Tetraphenylsiloles. Advanced Functional Materials, 2014, 24, 3621-3630.	7.8	123
97	Ultrafast Cr(vi) removal from polluted water by microwave synthesized iron oxide submicron wires. Chemical Communications, 2014, 50, 8036.	2.2	34
98	Stitching graphene oxide sheets into a membrane at a liquid/liquid interface. Chemical Communications, 2014, 50, 15944-15947.	2.2	26
99	Effects of preferred orientation on electrical properties of Mn1.56Co0.96Ni0.48O4±δspinel films. Materials Letters, 2014, 137, 36-40.	1.3	21
100	Rational Design of Aggregation-Induced Emission Luminogen with Weak Electron Donor–Acceptor Interaction to Achieve Highly Efficient Undoped Bilayer OLEDs. ACS Applied Materials & Interfaces, 2014, 6, 17215-17225.	4.0	113
101	Interfaceâ€5trengthened Polyimide/Carbon Nanofibers Nanocomposites with Superior Mechanical and Tribological Properties. Macromolecular Chemistry and Physics, 2014, 215, 1407-1414.	1.1	15
102	Metal nanoparticle-directed NiCo2O4 nanostructure growth on carbon nanofibers with high capacitance. Chemical Communications, 2014, 50, 8253.	2.2	27
103	Threeâ€Dimensional Nitrogen and Boron Coâ€doped Graphene for Highâ€Performance Allâ€Solidâ€State Supercapacitors. Advanced Materials, 2012, 24, 5130-5135.	11.1	1,270